Microstructural evolution in m-plane GaN growth on m-plane SiC

doi: 10.1063/1.2841671

Microstructural evolution in *m*-plane GaN growth on *m*-plane SiC

Qian Sun,[1,a)] Soon-Yong Kwon,[1] Zaiyuan Ren,[1] Jung Han,[1,b)] Takeyoshi Onuma,[2] Shigefusa F. Chichibu,[2] and Shaoping Wang[3]
[1]*Department of Electrical Engineering, Yale University, New Haven, Connecticut 06520, USA*
[2]*Institute of Multidisciplinary Research for Advanced Materials, Tohoku University, 2-1-1 Katahira, Aoba, Sendai 980-8577, Japan*
[3]*Fairfield Crystal Technology, LLC., 8 South End Plaza, New Milford, Connecticut 06776, USA*

(Received 1 December 2007; accepted 14 January 2008; published online 7 February 2008)

This letter presents a study on the nucleation and microstructural evolution of *m*-plane GaN epilayers on *m*-plane SiC substrates using high-temperature AlN buffer layers. Controlled growth interruptions were carried out to render snapshots of heteroepitaxial dynamics. It was discovered that island coalescence results in an inhomogeneous mosaic tilt along the *c*-axis. Mesoscopic study of nucleation evolution helps elucidate the origin of commonly observed surface undulation and striation, which is attributed to concave growth due to the coalescence of trapezoidal islands upon contact. A model correlating microstructural defects with optical properties is proposed to explain the observed pattern in spatially resolved cathodoluminescence mapping. © *2008 American Institute of Physics*. [DOI: 10.1063/1.2841671]

The reports of homoepitaxial growth of *m*-plane InGaN light-emitting diodes and laser diodes offer ample evidence to the efficacy of nonpolar III-nitrides devices.[1–4] Understanding of the nucleation and growth of nonpolar GaN on dissimilar substrates, nevertheless, remains a critical subject given the limited availability of large-area bulk GaN substrates. Heteroepitaxial growth of nonpolar GaN has revealed at least two major obstacles. The density of extended defects in nonpolar GaN (including threading dislocations and stacking faults[5]) is much higher than that in *c*-plane epilayers and exhibits an anisotropic nature.[6–8] Furthermore, the surface of nonpolar GaN layers frequently shows striation morphology with a substantial surface undulation perpendicular to the striation direction.[6,9] In contrast to the rich literature of *c*-plane GaN, very little has been reported regarding the heteroepitaxy of nonpolar GaN.[7] In this paper, we report an investigation of the nucleation and coalescence of *m*-plane GaN grown on *m*-plane 4*H*-SiC substrates. Correlation of the nucleation evolution with surface morphology, microstructure, and luminescence efficiency unveils the origin of commonly observed surface roughness and anisotropic mosaicity.

m-plane GaN was grown in a horizontal metalorganic chemical vapor deposition reactor. A 220 nm thick AlN buffer layer was deposited at 1150 °C with a V/III ratio of 780. The growth condition for *m*-plane GaN is modified based on the *c*-plane procedure at 300 mbars with a lower V/III ratio (~200) and a higher temperature (1070 °C) to achieve optically smooth surface. Mesoscopic sample morphology was studied by a scanning electron microscope (SEM) (FEI XL30 field-emission microscope). A four-axis x-ray diffractometer (Bede D1) was used to measure the x-ray rocking curves (XRCs) of the *m*-plane GaN films. Cathodoluminescence (CL) with monochromatic imaging was performed in a modified SEM at 100 K with an acceleration voltage of 5 kV and an e-beam current of 500 pA.

As-grown AlN buffer layers on SiC show a smooth surface and exhibit a narrow $(10\underline{1}0)$ XRC with a linewidth of ~0.1°. To understand the morphological and microstructural evolution for GaN growth, controlled interruptions were performed to obtain *m*-GaN with thicknesses of 30, 210, and 1100 nm for samples A, B, and C, respectively. For the thinnest sample (nominal thickness of ~30 nm, sample A), the surface exhibits a nonuniform coverage of GaN rod-shape islands with a majority aggregated along preexisting polishing scratches, as shown in the inset of Fig. 1(a). Atomic force microscope study of the surface of AlN buffers also shows random straight grooves replicating the polishing scratches of SiC substrate. The GaN islands aggregated along polishing scratches have proceeded into coalescence, while islands outside surface scratches are randomly and sparsely distributed. The nonuniform and incoherent nucleation behavior produces islands with varying density, size, and height [Fig. 1(a)]. At a thickness of 0.2 μm, sample B exhibits a mostly coalesced surface with a rough morphology, and pits can be observed as a result of incomplete coalescence [Fig. 1(b)]. Sample C shows a fully coalesced surface with stripelike features along the *a*-axis [Fig. 1(c)].

The mosaic tilt in the *m*-plane GaN films was studied by $(10\underline{1}0)$ XRCs measured under two different configurations with the in-plane *a*-axis (*a*-axis tilt) or the *c*-axis (*c*-axis tilt) within the x-ray scattering plane. (The *a*-axis tilt measures the mis-orientation from *m*-axis toward the in-plane *a*-axis.) For all the three samples with different thicknesses, the XRC for *a*-axis tilt measurement presents a single peak with a similar linewidth of ~0.3°. Figure 2(d) shows that of sample C as an example. In contrast, the thinnest GaN film, sample A, exhibits a weak and broad (~1.3°) peak for *c*-axis tilt [Fig. 2(a)]. As the growth proceeds, furthermore, a weak shoulder appears besides the main peak in the XRC for the *c*-axis tilt of sample B [Fig. 2(b)]. The appearing of the distinct shoulder indicates that there is an inhomogeneous mosaic tilt because a homogeneous mosaic tilt can only lead to peak broadening. Finally, for sample C, the shoulder in the XRC grows into a level comparable to and partially merged with the main peak [Fig. 2(c)]. The increasing weight of the

[a)]Electronic mail: qian.sun@yale.edu.
[b)]Electronic mail: jung.han@yale.edu.

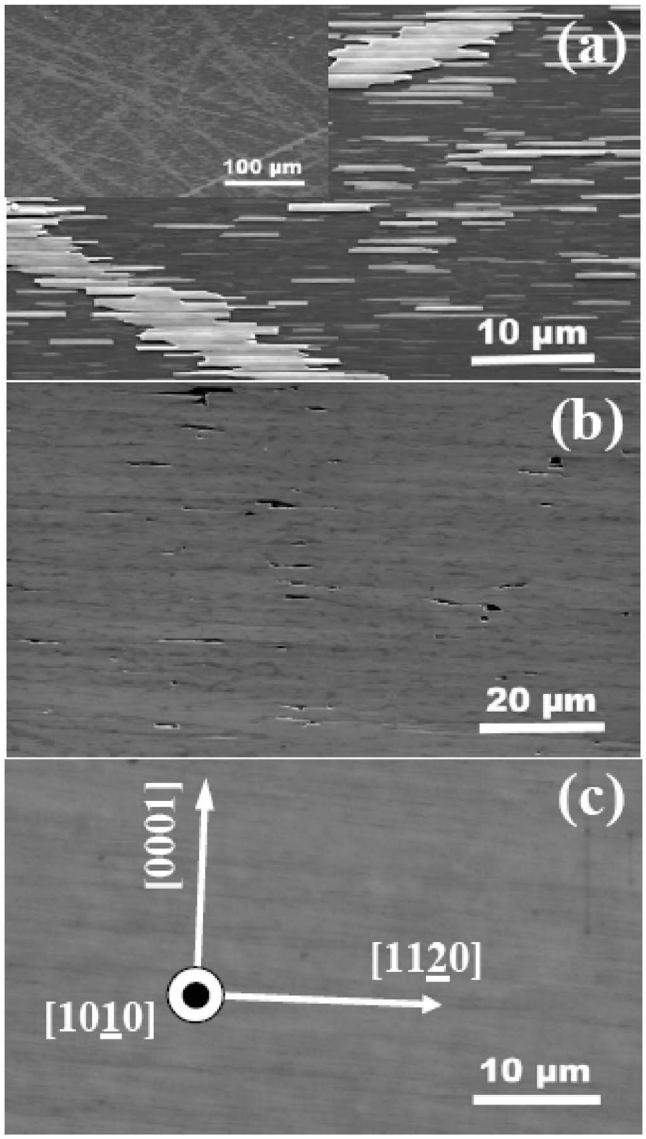

FIG. 1. Plan-view SEM images of samples (a) A, (b) B, and (c) C. The inset in (a) shows a broad view of sample A surface.

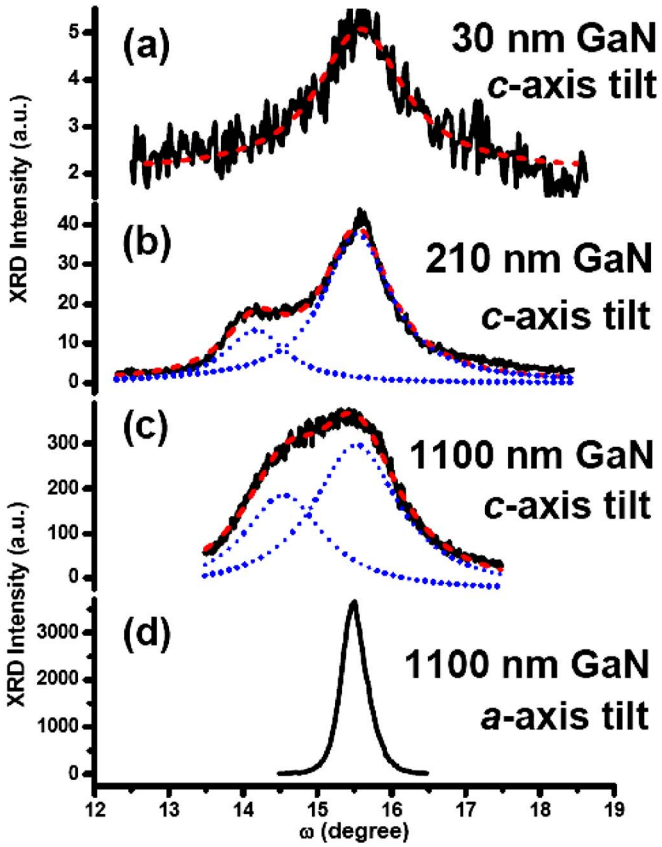

FIG. 2. (Color online) GaN (10$\bar{1}$0) x-ray rocking curves of (a) sample A, (b) sample B, and (c) sample C with the *c*-axis within the x-ray scattering plane; (d) sample C with the in-plane *a*-axis within the x-ray scattering plane. The red dash and blue dot lines are Lorentz fittings for the raw data.

inhomogeneously broadened peak implies that the inhomogeneous mosaic tilt propagates in the subsequently grown layer during and after coalescence. The above observation has clearly revealed that there is an anisotropic microstructural evolution during the *m*-plane GaN growth along the two in-plane axes.

For sample C, we notice a gradient in surface morphology within 1 mm of the wafer edge. Toward the wafer edge growth becomes less continuous from partial coalescence to isolated islands with a decreasing density [Fig. 3(a)]. Such a morphological variation is related to a gradient in V/III ratio due to the gas-phase diffusion of Ga source.[10] Two consequences of such a decreasing V/III ratio toward the edge are (i) a reduction in nucleation probability toward the edge[11] and (ii) a change in the shape of the island.[12] When properly interpreted, the spatial variation of the morphology in fact renders a panoramic record regarding the coalescence dynamics. As shown in Fig. 3(b), the isolated mesas near wafer edge are enclosed by three {10$\bar{1}$0}, three {10$\bar{1}$1} planes, and the (000$\bar{2}$) plane. The characteristic trapezoidal shape in plan-view images can be understood by Wulff's theorem with (000$\bar{2}$) and {10$\bar{1}$1} being the slowest growing planes.[12,13] When the trapezoidal faceted islands approach each other along the *c*-axis at the onset of coalescence, a vertical triangular concave gap is formed by (10$\bar{1}$1) and (000$\bar{2}$) planes [Fig. 3(c)]. Subsequent asymmetric coales-

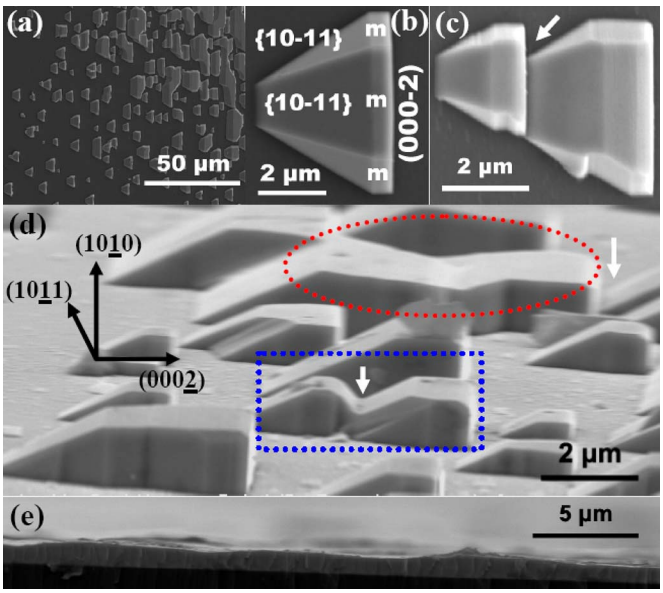

FIG. 3. (Color online) [(a)–(c)] Plan-view SEM images, (d) perspective view SEM image of sample C near-edge area, and (e) cross sectional view SEM image of sample C fully coalesced center area. The blue rectangular and red oval dotted lines in (d) mark out the regions with partial and full coalescence along the *c*-axis between adjacent mesas, respectively.

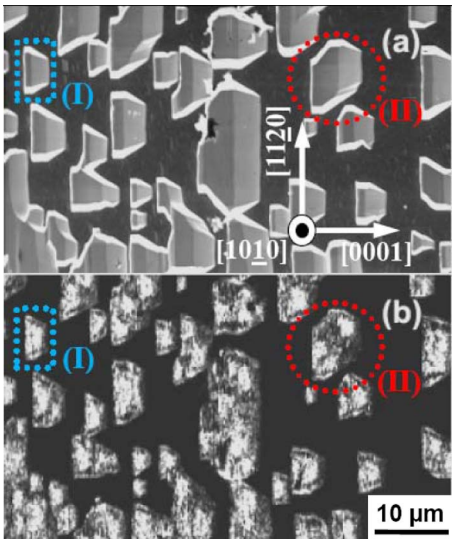

FIG. 4. (Color online) (a) Plan-view SEM image and (b) micro-CL monochromatic mapping collected at 380 nm of a near-edge area of sample C. The blue rectangular (I) and red circular (II) dotted lines mark out mesas with a trapezoidal and an irregular shape, respectively.

cence proceeds to fill the triangular gap [Fig. 3(d)] according to a *modified* Wulff's theorem for concave growth front where the surface geometry is dominated by *fast* growing planes.[13] It is worth noting that, due to a reduced in-plane symmetry, the concave growth during coalescence is further divided into the filling up of a vertical concave [arrowed region in Fig. 3(d)] and a horizontal concave [arrowed region in Fig. 3(c)]. By correlating the coalescence behavior at different stages [rectangular and oblong circles in Figs. 3(d) and 3(e)], we conclude that surface undulation along the *c*-axis is directly related to the filling of vertical concaves during coalescence [Fig. 3(d)], especially when the coalescing islands have different heights due to the nonuniform nucleation at the beginning. This surface undulation along the *c*-axis is a major contribution to surface roughness and striation [Fig. 3(e)]. It is noted that in the center of sample A surface (nominal thickness of ~30 nm), a similar coalescence behavior with a curved surface between adjacent short faceted GaN islands has also been clearly observed. Considering the inhomogeneous mosaic tilt emerging during coalescence process (Fig. 2), it is reasonable to assert that the filling up of vertical concaves is responsible for the observed asymmetric *c*-axis tilt. (The filling up of horizontal concaves might greatly contribute to mosaic twist, which needs a further careful study.) The asymmetric coalescence along the *c*-axis between (10$\bar{1}$1) and (000$\bar{2}$) planes may conceivably generate structural defects, such as threading dislocations and basal plane stacking faults.[7]

To elucidate the interplay between coalescence dynamics and microstructural properties, SEM imaging [Fig. 4(a)] with concurrent monochromatic CL mapping [Fig. 4(b)] was employed. Rectangle (I) encloses a single-crystalline trapezoidal island before coalescence with a relatively uniform CL emission across the entire island. For illustration purpose, a mesa with an irregular shape is marked out by circle (II) in Fig. 4. Although the SEM image [Fig. 4(a)] exhibits a homogeneous appearance for this irregular mesa, the micro-CL mapping shows an inhomogeneous contrast with a dark region between the two trapezoidal bright regions. It can be inferred that the island under viewing is derived from a coalescence of two original islands displaced along the *a*-axis. The coalescence regions (filling up of vertical and horizontal concaves) emit much fewer photons than the regions of the original islands, which accounts for the contrast in the micro-CL mapping. Therefore, the coalescence regions are more defective. An employment of bulk GaN wafers, a good control of nucleation uniformity, and a mesoscopic optimization of island evolution during coalescence will be crucial to improve the microstructural quality of *m*-plane GaN.

In summary, we have studied the nucleation and microstructural evolution of *m*-plane GaN grown on *m*-plane SiC substrates with high-temperature AlN buffer. A nonuniform and incoherent nucleation of GaN on AlN buffer is clearly observed. It is found that the surface undulation due to the asymmetric coalescence along the *c*-axis between (10$\bar{1}$1) and (000$\bar{2}$) planes is directly responsible for the significant roughness of *m*-plane GaN surface. Furthermore, XRC measurements combined with micro-CL mapping indicate that it is the asymmetric coalescence along the *c*-axis that gives rise to the inhomogeneous anisotropic mosaic tilt in *m*-plane GaN film.

The financial support for this work was partially provided by DOE-NSF project.

[1]M. C. Schmidt, K.-C. Kim, H. Sato, N. Fellows, H. Masui, S. Nakamura, S. P. DenBaars, and J. S. Speck, Jpn. J. Appl. Phys., Part 2 **46**, L126 (2007).
[2]K. Okamoto, H. Ohta, D. Nakagawa, M. Sonobe, J. Ichihara, and H. Takasu, Jpn. J. Appl. Phys., Part 2 **45**, L1197 (2006).
[3]K. Okamoto, H. Ohta, S. F. Chichibu, J. Ichihara, and H. Takasu, Jpn. J. Appl. Phys., Part 2 **46**, L187 (2007).
[4]M. C. Schmidt, K.-C. Kim, R. M. Farrell, D. F. Feezell, D. A. Cohen, M. Saito, K. Fujito, J. S. Speck, S. P. DenBaars, and S. Nakamura, Jpn. J. Appl. Phys., Part 2 **46**, L190 (2007).
[5]M. D. Craven, S. H. Lim, F. Wu, J. S. Speck, and S. P. DenBaars, Appl. Phys. Lett. **81**, 469 (2002).
[6]H. Wang, C. Chen, Z. Gong, J. Zhang, M. Gaevski, M. Su, J. Yang, and M. A. Khan, Appl. Phys. Lett. **84**, 499 (2004).
[7]M. D. Craven, F. Wu, A. Chakraborty, B. Imer, U. K. Mishra, S. P. DenBaars, and J. S. Speck, Appl. Phys. Lett. **84**, 1281 (2004).
[8]R. Armitage, M. Horita, J. Suda, and T. Kimoto, J. Appl. Phys. **101**, 033534 (2007).
[9]C. Q. Chen, M. E. Gaevski, W. H. Sun, E. Kuokstis, J. P. Zhang, R. S. Q. Fareed, H. M. Wang, J. W. Yang, G. Simin, M. A. Khan, H. P. Maruska, D. W. Hill, M. M. C. Chou, and B. H. Chai, Appl. Phys. Lett. **81**, 3194 (2002).
[10]C. C. Mitchell, M. E. Coltrin, and J. Han, J. Cryst. Growth **222**, 144 (2001).
[11]T. Yang, K. Uchida, T. Mishima, J. Kasai, and J. Gotoh, Phys. Status Solidi A **180**, 45 (2000).
[12]K. Hiramatsu, K. Nishiyama, A. Motogaito, H. Miyake, Y. Iyechika, and T. Maeda, Phys. Status Solidi A **176**, 535 (1999).
[13]D. Du, D. J. Srolovitz, M. E. Coltrin, and C. C. Mitchell, Phys. Rev. Lett. **95**, 155503 (2005).